

Spatial-Mode Quantum Cryptography in a 545-Dimensional Hilbert Space

Lukas Scarfe,^{1,2,3,*} Yingwen Zhang,^{1,2,3,†} and Ebrahim Karimi^{1,2,3,4}

¹*Nexus for Quantum Technologies, University of Ottawa, Ottawa ON Canada, K1N6N5*

²*National Research Council of Canada, 100 Sussex Drive, Ottawa ON Canada, K1A0R6*

³*Joint Centre for Extreme Photonics, National Research Council and University of Ottawa, Ottawa, Ontario, Canada*

⁴*Institute for Quantum Studies, Chapman University, Orange, California 92866, USA*

A major challenge in quantum key distribution (QKD) with spatial modes lies in efficiently generating, manipulating, and detecting high-dimensional quantum states. Here, we present a hybrid QKD protocol that integrates entanglement-based and prepare-and-measure approaches, utilizing position and momentum correlations of photon pairs generated via spontaneous parametric downconversion. Through projective measurements on one photon, the sender remotely prepares spatial modes at the receiver’s end, simplifying state preparation. Detection is enhanced using advanced event-based single-photon cameras. Our scheme supports QKD in a 545-dimensional Hilbert space—the highest reported for spatial encoding—achieving 5.07 bits per coincidence in an optimized 90-mode configuration. This work demonstrates a scalable route to high-dimensional, spatially encoded quantum communication.

I. INTRODUCTION

Entanglement between two or more particles is one of the most profound concepts in quantum theory, forming the cornerstone of both foundational investigations and emerging quantum technologies [1]. On a conceptual level, entanglement challenges our classical understanding of nature, raising fundamental questions about the nature of reality and the principle of locality. From a technological perspective, entanglement serves as the primary resource, enabling capabilities beyond those of classical systems, including quantum computing [2, 3], advanced sensing techniques [4–6], quantum teleportation [7, 8], and secure communication protocols [9, 10]. Of the aforementioned technologies, quantum communications, in particular quantum key establishment or distribution (QKD), is primed to be one of the first quantum technologies to reach maturity and be implemented in wide-scale deployments [11]. This allows individuals to communicate with absolute certainty of privacy over the quantum internet, provided that the observed error rate on the communication channel remains below a known threshold. There are two main types of QKD protocols: prepare-and-measure [12] and entanglement-based [13]. In the former, one party (commonly referred to as Alice) prepares single photons in randomly chosen quantum states and transmits them to the receiving party (Bob). This process must be truly random, requiring a quantum random number generator (QRNG) and very precise control over the generation and manipulation of quantum states to ensure the protocol’s security and efficiency. Entanglement-based QKD protocols, on the other hand, have their randomness inherently built in. The generation of entangled photons, most often through sponta-

neous parametric downconversion (SPDC), is a random process where the output photon pair can be entangled in multiple degrees of freedom [14]. Entanglement-based QKD can also allow Alice and Bob to double the distance over which they can exchange keys by having the photon source in between them [15].

The increase in distance between sender and receiver has been the main benefit of entanglement QKD protocols [16], namely for fibre-based quantum channels. However, here, we seek to utilize it differently. We consider the case where Alice is the source of the entangled photons, and therefore, Alice and Bob do not need to consider the photon source being potentially compromised. After generating the entangled photons, Alice performs a projective measurement in one of the two chosen mutually unbiased bases (MUB) on the idler photon, and sends the signal photon to Bob. This implementation behaves like a prepare-and-measure scheme but employs an entangled source. The benefit of using the entangled source this way is that Alice can rapidly generate or “prepare” high-dimensional modes simply by performing a local measurement. QKD, when implemented in high dimensions, can allow for higher information density per photon [17], as well as an increased error tolerance [18, 19] but is limited by the difficulty in generating and detecting the high-dimensional modes. While using higher dimensions has been a large interest in the field of research [20–22], traditional qubit-based protocols remain the focus of attempts to bring QKD to the mainstream [23, 24] thanks to the relative simplicity of generating and detecting 2-dimensional polarization modes.

By allowing Alice to “prepare” Bob’s photon via a local measurement process, the challenge of generating high-dimensional modes is significantly reduced. The detection challenges are also significantly reduced with the advent of event-based time-tagging single-photon cameras that have been developed over recent years [25, 26]. In this work, we use the conjugate properties of position and momentum of a photon pair generated through SPDC [27]. We show that with this method, we can

* lscar039@uottawa.ca; These authors contributed equally to this work

† yzhang6@uottawa.ca; These authors contributed equally to this work

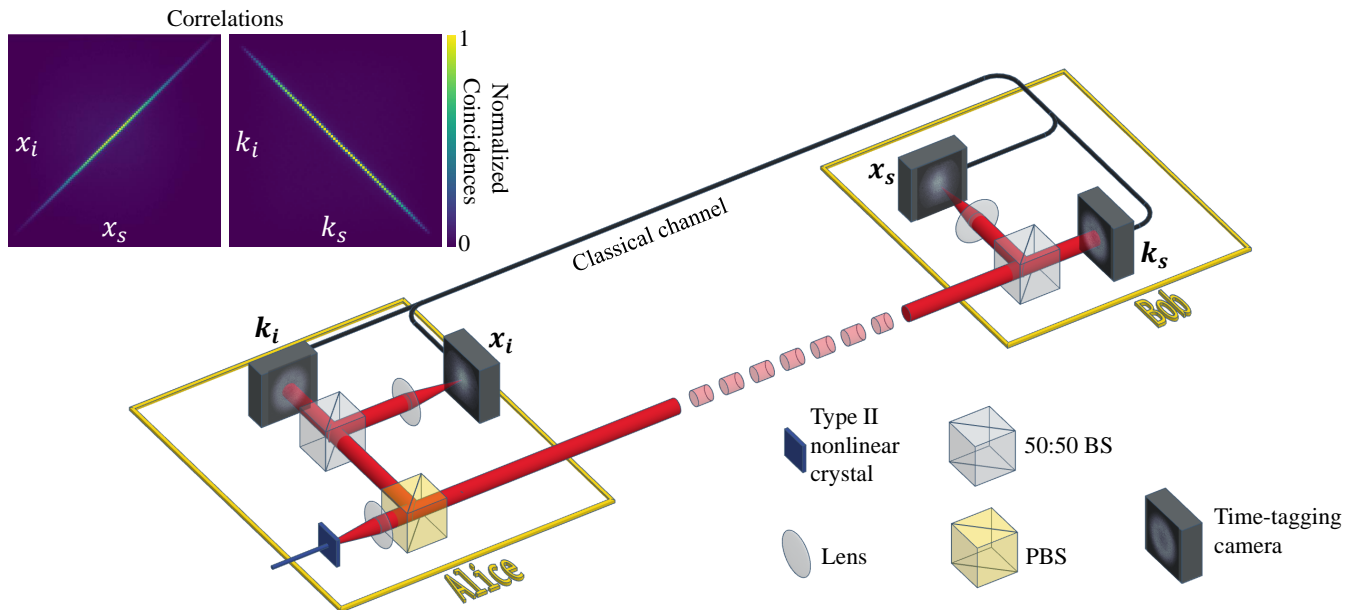


FIG. 1. **Conceptual setup for position-momentum QKD.** Position-momentum entangled photon pairs with orthogonal polarization are created via Type-II SPDC by Alice who keeps the vertically polarized idler photon locally and sends the horizontally polarized signal photon to “Bob”. For detection at the two parties, the photons are randomly split to be measured in one of the two MUBs, either in position or momentum, by time-tagging cameras. Finally, the two parties compare their measurement bases via a classical channel to create their secret key. Inset on the top left shows the measured position and momentum correlations in the horizontal direction. Correlations in the vertical direction looks near identical to that of the horizontal direction.

generate distinct modes capable of supporting QKD up to a 545-dimensional Hilbert space. While not a record for any degree of freedom [28], as far as we are aware, this is the highest dimensionality yet achieved for spatial encoding, and can potentially be further increased by considering the additional degree of freedom of time of arrival or time-bins [29]. This high number of dimensions leads to a high error rate and we find the best-performing configuration in terms of information density to be 90 modes in position (x) and momentum (k) allowing for 5.07 bits per photon coincidence. We also consider the effects of different orderings of the optical modes on performance due to the contrast between our cartesian-based measurement device, and the cylindrical symmetry of the propagating beams.

II. METHODS

A. Experimental Design

The conceptual setup for realizing very high-dimensional QKD via position-momentum entangled photons is shown in Figure 1. High-dimensional position-momentum entangled photon pairs with orthogonal polarization are created via Type-II SPDC by Alice. Using a polarizing beamsplitter (PBS), the vertically po-

larized idler photon is kept locally by Alice and the horizontally polarized signal photon is sent to Bob. At both ends, the quantum states of the photons are randomly measured in one of two mutually unbiased bases (MUB)—either position or momentum—using time-tagging cameras. Rather than using external random number generators, the randomness in the position and momentum mode of the photon pair is naturally given by their position-momentum entanglement and the randomness of the MUB selection is achieved using 50:50 beam splitters (50:50 BS). Finally, over a classical channel, Alice and Bob compare and identify the matching bases in their measurement to form a shared secret key, and apply error correction and privacy amplification to ensure security. A detailed experimental setup can be found in the Supplementary Materials.

The expected correlation widths in position δ_x and momentum δ_k can be approximated according to [30, 31]:

$$\delta_k \approx 1/(2\sigma_p) \quad \delta_x \approx \sqrt{\frac{2\alpha L\lambda_p}{\pi}}, \quad (1)$$

where σ_p is the pump beam width, L is the crystal length, λ_p is the pump wavelength, and $\alpha = 0.455$ is a constant factor from the Gaussian approximation of the sinc phase matching function. Thus, to achieve very high-dimensional position-momentum entanglement, a collimated pump laser, with a large beam waist, should be

used to pump a thin nonlinear crystal in order to ensure high position and momentum correlation. For this experiment, $L = 1$ mm, $\lambda_p = 405$ nm and $\sigma_p = 0.12$ mm (0.28 mm FWHM). Our σ_p is limited by the transverse dimension of the crystal, which is $1 \text{ mm} \times 2 \text{ mm}$.

We measured a correlation width of $\delta_k = 5.5 \times 10^{-3} \mu\text{m}^{-1}$ and $\delta_x = 8.4 \mu\text{m}$ (Figure 1 inset), this is in rough agreement with the approximate correlation width of $\delta_k = 4.2 \times 10^{-3} \mu\text{m}^{-1}$ and $\delta_x = 11 \mu\text{m}$ as given by (1).

For our system, a singles rate of $760 \times 10^3/\text{s}$ and a coincidence rate of $38 \times 10^3/\text{s}$ was measured by the camera. For the results presented in the following sections, a data acquisition time of 100 seconds was used.

B. Quantum key distribution analysis

We consider the position basis x and the momentum basis k as conjugate variables, linking via a Fourier transform, and therefore mutually unbiased [32]. When the idler photon is projected onto one of these bases, information is gained about the state of the signal photon in that same basis, but lost in the conjugate basis. We exploit this property to investigate how the position and momentum of photon pairs generated via SPDC can be used in quantum key distribution.

The simplest entanglement-based QKD protocol to consider is the high-dimensional BB84 protocol [9]. When implemented with entangled photon sources, it is often referred to as the BBM92 protocol [33]. In this protocol, two mutually unbiased bases are used, each consisting of d modes that define the dimensionality of the scheme. When the signal and idler photons are measured in the same basis by Bob and Alice, respectively, they are expected—due to entanglement—to yield the same outcome. A mismatch in their outcomes indicates an error, which may have been introduced by a potential eavesdropper. By monitoring the error rate and setting an acceptable threshold, Alice and Bob can ensure the establishment of a secure key. Measurements performed in different bases do not convey useful information and are discarded during the sifting process. High-dimensional QKD has a well-defined error tolerance, which increases with the dimensionality of the protocol. After sifting—where only measurement outcomes in the same basis are retained—the final amount of information encoded per photon is given by [34]:

$$R(e) = \log_2(d) - 2h_d(e), \quad (2)$$

where e is the quantum dit error rate (QDER) and $h_d(e) = -\log_2(e/(d-1)) - (1-e)\log_2(1-e)$ is the high-dimensional equivalent of the Shannon Entropy. By setting (2) equal to zero and solving for e , one can find the security threshold above which any additional errors would lead to an insecure channel in which no keys can be exchanged.

In order to calculate QDER, one must measure the probability of detection matrix when Alice and Bob mea-

sure in the same basis. This detection matrix describes the probability that Bob will measure a particular state, given the state in which Alice’s photon is measured. With this matrix ($C_{x,k}$), one can find the QDER as follows,

$$e = 1 - \frac{1}{d} \text{Tr}(C_{x,k}). \quad (3)$$

III. RESULTS

A. Mode Orderings

To evaluate the impact of mode structure and spatial arrangement on the performance of a quantum key distribution (QKD) protocol, we performed a sub-sampling of the total number of pixels available in our detector. This approach allowed us to investigate how different spatial mode orderings and inter-mode spacing influence the system’s error rates and overall performance. Specifically, we examined three distinct configurations: (1) a Cartesian grid pattern aligned with the native pixel layout of the detector, (2) an angled-grid pattern rotated by 45° relative to the detector’s orientation, and (3) a hexagonal layout, known for its efficient packing within circular apertures.

Figure 2 shows the crosstalk measurements for three different pixel-mode configurations with dimensions $d = 4$, $d = 90$, and $d = 545$. The corresponding quantum dit error rates (QDER) were measured to be $e = 0$, $e = 5.95\%$ and $e = 31.8\%$, respectively, resulting in secret key rates of $R(e) = 2, 5.07$, and 1.51 bits per photon. These results highlight how increasing the dimensionality can lead to higher error rates due to increased mode overlap and crosstalk. Our initial hypothesis was that the hexagonal mode arrangement would outperform the other layouts by allowing denser and more uniform packing of spatial modes within the circular detection aperture. This was expected to reduce inter-mode crosstalk and consequently lower the QDER. The three mode orderings—Cartesian grid aligned with the detector pixels, a hexagonal grid, and a grid rotated by 45° —are shown in the insets of Figure 2, where each white dot indicates a pixel used as a spatial mode.

Contrary to our expectations, however, no particular layout demonstrated a clear advantage over the others. As shown in Figure 3, all three configurations yielded comparable error rates when tested at similar dimensionalities. This suggests that, within the regime tested, the specific ordering of spatial modes does not significantly impact QKD performance, and other factors—such as inter-mode spacing or detector noise—may play a more critical role.

B. Modes vs Error

The crosstalk matrices shown in Figure 2 represent the detection probability distributions $C_{x,k}$ across differ-

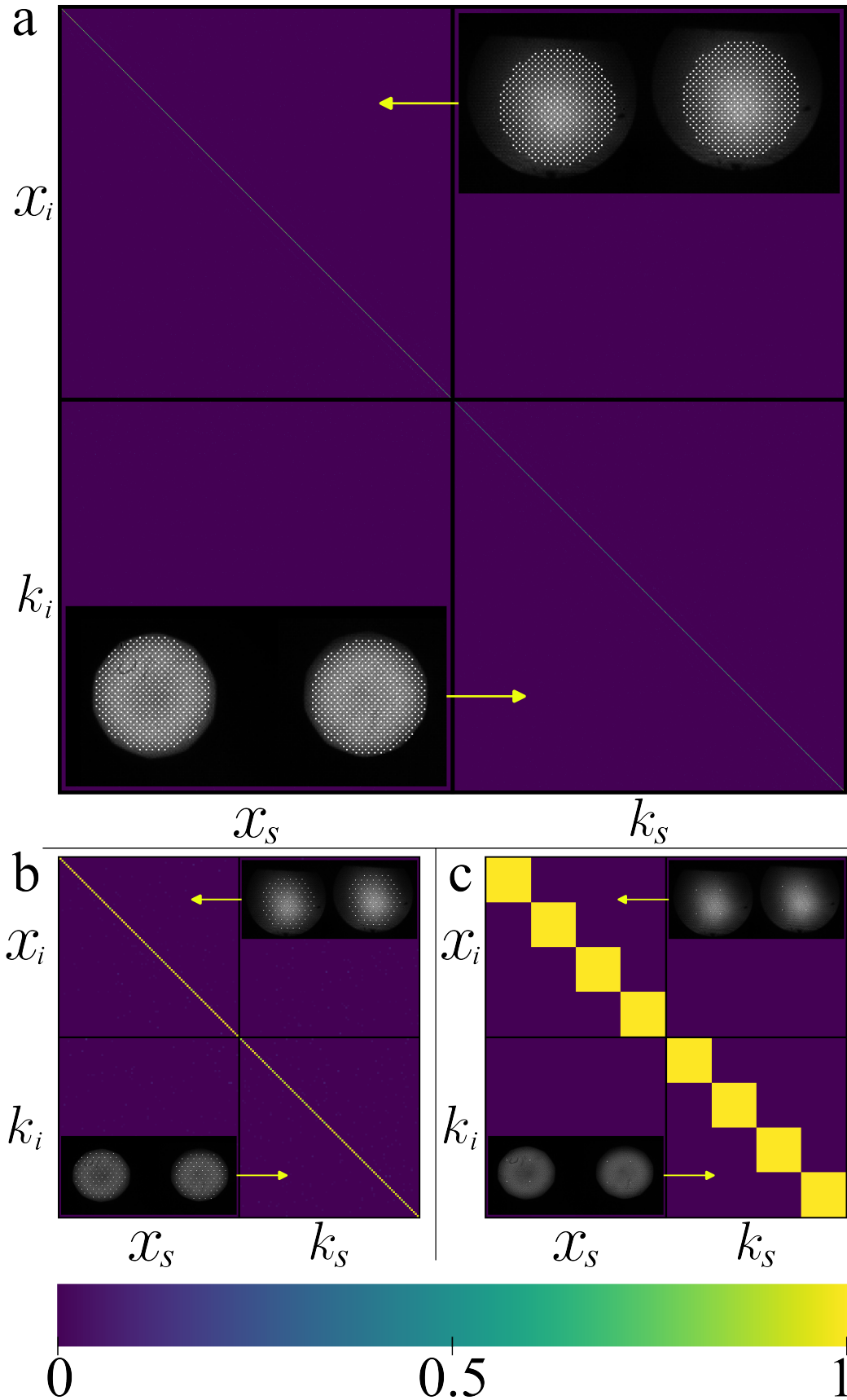


FIG. 2. **Crosstalk plots for differing dimensions, $C_{x,k}$.** Each pixel that is used as a mode is highlighted with white in the insets of the crosstalk arrays. a) Crosstalk array of the highest achieved dimension in which QKD could still be achieved in the channel $d = 545$, $e = 31.8\%$, $R(e) = 1.51$ bits/photon. This was achieved using a grid-shaped mode ordering rotated 45° . b) Crosstalk array of mode ordering which had the highest sifted key rate, $d = 90$, $e = 5.95\%$, $R(e) = 5.07$ bits/photon. The modes were ordered in a hexagonal grid shape. c) Crosstalk array of the lowest error rate $d = 4$, $e = 0$, $R(e) = 2$ bits/photon. In this case, the modes were ordered in a grid shape aligned with the detectors' pixels.

ent dimensionalities. In an ideal scenario with no errors, when Alice and Bob measure in the same basis—either (x_i, x_s) or (k_i, k_s) —the detection probability would be unity along the diagonal elements and zero elsewhere. In our implementation, each spatial mode corresponds to an individual pixel on the detector. However, this approach utilizes only a small fraction of the detector’s active area. In the best case, just 12.7% of the available 4293 pixels are used as modes. As a result, when Alice and Bob choose opposite measurement bases, the probability of both photons landing on predefined mode pixels is low—with the probability proportional to $(d/4293)^2$ for any dimension d , assuming uncorrelated detection positions. Conversely, when both parties measure in the same basis, a photon detected on a mode pixel by Alice is highly likely to have its pair detected on the corresponding mode pixel by Bob.

As the protocol’s dimensionality increases, the spatial separation between neighboring modes decreases, leading to greater overlap and an increase in cross-talk errors. Consequently, the quantum dit error rate rises with dimension. Despite this, the sifted key rate initially increases with dimensionality and peaks at $d = 90$, suggesting this to be the system’s optimal operating point in terms of balancing key rate and error performance.

The optimal operating dimension of the QKD system is fundamentally linked to the number of spatial modes—or the Schmidt number—of the SPDC source. This number characterizes the intrinsic entanglement dimensionality of the photon pairs generated and is determined by the properties of the nonlinear crystal and the spatial and spectral characteristics of the pump laser. In essence, the Schmidt number sets an upper bound on the number of usable orthogonal modes. Therefore, to reliably implement QKD at higher dimensions, it is necessary to employ an SPDC source with a correspondingly higher Schmidt number, which will require engineering both the crystal and the pump conditions appropriately based on (1). The Schmidt number for position-momentum entanglement is given by $K = \frac{1}{4}(\delta_k \delta_x + \frac{1}{\delta_k \delta_x})^2$ [31], which for the measured δ_x and δ_k of our system gives $K = 118$.

IV. DISCUSSION

In this work, we explored the advantages of integrating an entangled photon source into a hybrid quantum key distribution (QKD) system that combines features of both entanglement-based and prepare-and-measure protocols. Our implementation leverages the transverse spatial degrees of freedom—specifically position and momentum—to encode information in high-dimensional quantum states. We demonstrated the ability to passively generate quantum states residing in Hilbert spaces of up to 545 dimensions while maintaining reliable quantum communication between two parties. This high-dimensional encoding not only enhances the robustness and security of the QKD system but also significantly

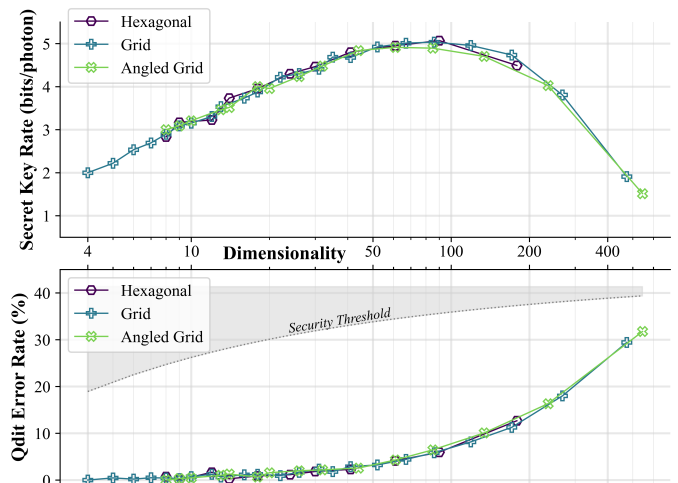


FIG. 3. **Effect of increased dimensions on the sifted key rate and the Qdit error rate (QDER).** Above) Plot of the sifted key rate vs dimension. Below) Plot of the QDER vs dimension. Different mode orderings are shown to perform similarly for error rate and subsequently key rate in all dimensions up to $d = 545$. The maximum error rate at which QKD could theoretically be implemented for each dimension is shown in the gray area of the lower plot and is denoted as the “Security Threshold”.

improves its information capacity. Notably, we achieved an information density of 5.07 bits per photon using a 90-dimensional protocol, thereby demonstrating a substantial increase in channel capacity compared to traditional two-dimensional approaches. While our efforts have focused on maximizing the number of accessible spatial modes in the system, we have not simultaneously optimized the total number of detected photon pairs. As previously discussed, our approach assigns only one pixel per mode, which inherently limits the number of usable coincidence events—particularly in lower-dimensional protocols. For example, in the case of a 4-dimensional implementation, out of the approximately 3.8 million total photon pairs recorded over a 100-second data acquisition window, only 278 pairs contributed to key generation. This low yield could be improved by increasing the spatial extent of each mode, thereby encompassing more pixels per mode; however, this comes at the cost of higher cross-talk and increased error rates due to reduced spatial separation between adjacent modes. In contrast, for higher-dimensional implementations such as the 545-dimensional case, the increased mode density led to 52,726 photon pairs contributing to key generation, demonstrating the advantage of working in larger Hilbert spaces. One straightforward approach to increase the detected pair rate in lower dimensions is to reduce mode overlap by engineering the pump beam and nonlinear crystal parameters to increase the Schmidt number. This would lead to a broader range of distinguishable modes and more effective use of the camera pixels. Another sig-

nificant limiting factor is the quantum efficiency of the single-photon camera used in our experiment, which is currently only about 8% [35]. With recent and ongoing advancements in single-photon imaging technologies [36], we anticipate that this limitation will be significantly alleviated in the near future, enabling higher detection rates and more efficient key generation across all dimensionalities.

Due to the non-uniform intensity distribution of the photons in both position bases, the detected spatial modes exhibit varying count rates, leading to an imbalance in the number of events per mode. This non-uniformity can be partially addressed during the sifting process by normalizing the detection counts—specifically, by discarding events from modes with higher count rates to equalize the contribution across all modes. However, this approach sacrifices valuable data. A more efficient alternative could involve designing or selecting spatial mode shapes that inherently produce uniform count rates across the modes, thereby maximizing the utilization of all detected events. Such an optimization could enhance the efficiency of QKD protocols using the position (x) and momentum (k) degrees of freedom derived from spontaneous parametric down-conversion (SPDC) sources. The observed count distribution is intrinsically linked to the phase-matching conditions of the nonlinear crystal used in the SPDC process. This typically results in a configuration where fewer pixels are needed to define modes near the center of the distribution, while modes in the periphery require binning of a larger number of pixels—assuming that counts are uniform for both regions’ modes. Optimizing the spatial mode definitions in this way could not only improve mode uniformity but might also reduce cross-talk between neighboring modes—further increasing the fidelity of the key distribution process.

Another promising avenue for future research involves exploring spatial modes beyond the pixel basis, such as shape-invariant modes like Laguerre-Gauss and Hermite-Gauss modes. These modes benefit from well-established spatial mode sorting techniques [37–40], which can provide a robust and scalable framework for high-dimensional quantum communication [41]. A com-

parative study between the performance of pixel-based modes and analytically defined spatial modes in terms of channel capacity, error rates, and experimental practicality would be of considerable value.

We anticipate that this hybrid entanglement / prepare-and-measure approach can be represented in other degrees of freedom, such as Laguerre-Gauss modes [42, 43], where the fast and efficient generation and detection of such modes in high dimensions is typically more challenging. In particular, we envision that this technique could serve as a foundation for rapidly generating and detecting LG modes, a well-established platform for high-dimensional QKD [41, 44], and thus further enhance the capacity and security of quantum communication networks.

FUNDING

This work was supported by Canada Research Chairs; National Research Council of Canada High-Throughput and Secure Networks (HTSN) Challenge Program; and the Alliance Consortia Quantum Grant (QUINT, ARAQNE).

ACKNOWLEDGEMENTS

The authors wish to express their sincere gratitude to Dr. Alessio D’Errico for his insightful discussions, careful reading of the manuscript, and valuable feedback and comments.

DISCLOSURES

The authors declare no conflicts of interest.

DATA AVAILABILITY

Data underlying the results presented in this paper are not publicly available at this time but may be obtained from the authors upon reasonable request.

-
- [1] R. Horodecki, P. Horodecki, M. Horodecki, and K. Horodecki, Quantum entanglement, *Rev. Mod. Phys.* **81**, 865 (2009).
- [2] H. Aghaee Rad, T. Ainsworth, R. N. Alexander, B. Altieri, M. F. Askarani, R. Baby, L. Bianchi, B. Q. Baragiola, J. E. Bourassa, R. S. Chadwick, I. Charania, H. Chen, M. J. Collins, P. Contu, N. D’Arcy, G. Dauphinais, R. De Prins, D. Deschenes, I. Di Luch, S. Duque, P. Edke, S. E. Fayer, S. Ferracin, H. Ferretti, J. Gefaell, S. Glancy, C. González-Arciniegas, T. Grainge, Z. Han, J. Hastrup, L. G. Helt, T. Hillmann, J. Hundal, S. Izumi, T. Jaeken, M. Jonas, S. Kocsis, I. Krasnokutska, M. V. Larsen, P. Laskowski, F. Laudenbach, J. Lavoie, M. Li,

- E. Lomonte, C. E. Lopetegui, B. Luey, A. P. Lund, C. Ma, L. S. Madsen, D. H. Mahler, L. Mantilla Calderón, M. Menotti, F. M. Miatto, B. Morrison, P. J. Nadkarni, T. Nakamura, L. Neuhaus, Z. Niu, R. Noro, K. Papirov, A. Pesah, D. S. Phillips, W. N. Plick, T. Rogalsky, F. Rortais, J. Sabines-Chesterking, S. Safavi-Bayat, E. Sazhaev, M. Seymour, K. Rezaei Shad, M. Silverman, S. A. Srinivasan, M. Stephan, Q. Y. Tang, J. F. Tasker, Y. S. Teo, R. B. Then, J. E. Tremblay, I. Tzitrin, V. D. Vaidya, M. Vasmer, Z. Vernon, L. F. S. S. M. Villalobos, B. W. Walshe, R. Weil, X. Xin, X. Yan, Y. Yao, M. Zamani Abnili, and Y. Zhang, Scaling and networking a modular photonic quantum computer, *Nature* **638**, 912

- (2025).
- [3] M. Foss-Feig, S. Ragole, A. Potter, J. Dreiling, C. Figgatt, J. Gaebler, A. Hall, S. Moses, J. Pino, B. Spaun, B. Neyenhuis, and D. Hayes, Entanglement from tensor networks on a trapped-ion quantum computer, *Phys. Rev. Lett.* **128**, 150504 (2022).
 - [4] S. Pirandola, B. R. Bardhan, T. Gehring, C. Weedbrook, and S. Lloyd, Advances in photonic quantum sensing, *Nature Photonics* **12**, 724 (2018).
 - [5] S. S. Szigeti, O. Hosten, and S. A. Haine, Improving cold-atom sensors with quantum entanglement: Prospects and challenges, *Applied Physics Letters* **118**, 140501 (2021), <https://pubs.aip.org/aip/apl/article-pdf/doi/10.1063/5.0050235/20022279/140501.1.5.0050235.pdf>.
 - [6] Q. Zhuang, Z. Zhang, and J. H. Shapiro, Distributed quantum sensing using continuous-variable multipartite entanglement, *Phys. Rev. A* **97**, 032329 (2018).
 - [7] Q.-C. Sun, Y.-L. Mao, S.-J. Chen, W. Zhang, Y.-F. Jiang, Y.-B. Zhang, W.-J. Zhang, S. Miki, T. Yamashita, H. Terai, X. Jiang, T.-Y. Chen, L.-X. You, X.-F. Chen, Z. Wang, J.-Y. Fan, Q. Zhang, and J.-W. Pan, Quantum teleportation with independent sources and prior entanglement distribution over a network, *Nature Photonics* **10**, 671 (2016).
 - [8] D. Bouwmeester, J.-W. Pan, K. Mattle, M. Eibl, H. Weinfurter, and A. Zeilinger, Experimental quantum teleportation, *Nature* **390**, 575 (1997).
 - [9] C. H. Bennett and G. Brassard, Quantum cryptography: Public key distribution and coin tossing, *Theoretical Computer Science* **560**, 7 (2014), *theoretical Aspects of Quantum Cryptography – celebrating 30 years of BB84*.
 - [10] Y. Li, W.-Q. Cai, J.-G. Ren, C.-Z. Wang, M. Yang, L. Zhang, H.-Y. Wu, L. Chang, J.-C. Wu, B. Jin, H.-J. Xue, X.-J. Li, H. Liu, G.-W. Yu, X.-Y. Tao, T. Chen, C.-F. Liu, W.-B. Luo, J. Zhou, H.-L. Yong, Y.-H. Li, F.-Z. Li, C. Jiang, H.-Z. Chen, C. Wu, X.-H. Tong, S.-J. Xie, F. Zhou, W.-Y. Liu, Y. Ismail, F. Petruccione, N.-L. Liu, L. Li, F. Xu, Y. Cao, J. Yin, R. Shu, X.-B. Wang, Q. Zhang, J.-Y. Wang, S.-K. Liao, C.-Z. Peng, and J.-W. Pan, Microsatellite-based real-time quantum key distribution, *Nature* 10.1038/s41586-025-08739-z (2025).
 - [11] M. Stanley, Y. Gui, D. Unnikrishnan, S. Hall, and I. Fattadin, Recent progress in quantum key distribution network deployments and standards, *Journal of Physics: Conference Series* **2416**, 012001 (2022).
 - [12] M. Sisodia and J. Ghosh, Prepare-and-measure based qkd protocol under free-space losses, *Physics Open* **17**, 100184 (2023).
 - [13] S. Ecker, J. Pseiner, J. Piris, and M. Bohmann, Advances in entanglement-based QKD for space applications, in *International Conference on Space Optics – ICSO 2022*, Vol. 12777, edited by K. Minoglou, N. Karafolas, and B. Cugny, International Society for Optics and Photonics (SPIE, 2023) p. 1277727.
 - [14] D. N. Klyshko, Coherent Photon Decay in a Nonlinear Medium, *ZhETF Pisma Redaktsiiu* **6**, 490 (1967).
 - [15] V. Zapatero, T. van Leent, R. Arnon-Friedman, W.-Z. Liu, Q. Zhang, H. Weinfurter, and M. Curty, Advances in device-independent quantum key distribution, *npj Quantum Information* **9**, 10 (2023).
 - [16] E. Waks, A. Zeevi, and Y. Yamamoto, Security of quantum key distribution with entangled photons against individual attacks, *Phys. Rev. A* **65**, 052310 (2002).
 - [17] H. Bechmann-Pasquinucci and W. Tittel, Quantum cryptography using larger alphabets, *Phys. Rev. A* **61**, 062308 (2000).
 - [18] S. Ecker, F. Bouchard, L. Bulla, F. Brandt, O. Kohout, F. Steinlechner, R. Fickler, M. Malik, Y. Guryanova, R. Ursin, and M. Huber, Overcoming noise in entanglement distribution, *Phys. Rev. X* **9**, 041042 (2019).
 - [19] N. J. Cerf, M. Bourennane, A. Karlsson, and N. Gisin, Security of quantum key distribution using d -level systems, *Phys. Rev. Lett.* **88**, 127902 (2002).
 - [20] A. Sit, F. Bouchard, R. Fickler, J. Gagnon-Bischoff, H. Larocque, K. Heshami, D. Elser, C. Peuntinger, K. Günthner, B. Heim, C. Marquardt, G. Leuchs, R. W. Boyd, and E. Karimi, High-dimensional intracity quantum cryptography with structured photons, *Optica* **4**, 1006 (2017).
 - [21] F. Bouchard, K. Heshami, D. England, R. Fickler, R. W. Boyd, B.-G. Englert, L. L. Sánchez-Soto, and E. Karimi, Experimental investigation of high-dimensional quantum key distribution protocols with twisted photons, *Quantum* **2**, 111 (2018).
 - [22] L. Scarfe, F. Hufnagel, M. F. Ferrer-Garcia, A. D’Errico, K. Heshami, and E. Karimi, Fast adaptive optics for high-dimensional quantum communications in turbulent channels, *Communications Physics* **8**, 79 (2025).
 - [23] J. F. Dynes, I. Choi, A. W. Sharpe, A. R. Dixon, Z. L. Yuan, M. Fujiwara, M. Sasaki, and A. J. Shields, Stability of high bit rate quantum key distribution on installed fiber, *Opt. Express* **20**, 16339 (2012).
 - [24] S.-K. Liao, W.-Q. Cai, W.-Y. Liu, L. Zhang, Y. Li, J.-G. Ren, J. Yin, Q. Shen, Y. Cao, Z.-P. Li, F.-Z. Li, X.-W. Chen, L.-H. Sun, J.-J. Jia, J.-C. Wu, X.-J. Jiang, J.-F. Wang, Y.-M. Huang, Q. Wang, Y.-L. Zhou, L. Deng, T. Xi, L. Ma, T. Hu, Q. Zhang, Y.-A. Chen, N.-L. Liu, X.-B. Wang, Z.-C. Zhu, C.-Y. Lu, R. Shu, C.-Z. Peng, J.-Y. Wang, and J.-W. Pan, Satellite-to-ground quantum key distribution, *Nature* **549**, 43 (2017).
 - [25] A. Nomerotski, Imaging and time stamping of photons with nanosecond resolution in timepix based optical cameras, *Nuclear Instruments and Methods in Physics Research Section A: Accelerators, Spectrometers, Detectors and Associated Equipment* **937**, 26 (2019).
 - [26] <https://www.amscins.com/product/chronos-series/phoebe>.
 - [27] M. P. Almeida, S. P. Walborn, and P. H. Souto Ribeiro, Experimental investigation of quantum key distribution with position and momentum of photon pairs, *Phys. Rev. A* **72**, 022313 (2005).
 - [28] T. Zhong, H. Zhou, R. D. Horansky, C. Lee, V. B. Verma, A. E. Lita, A. Restelli, J. C. Bienfang, R. P. Mirin, T. Gerrits, et al., Photon-efficient quantum key distribution using time-energy entanglement with high-dimensional encoding, *New Journal of Physics* **17**, 022002 (2015).
 - [29] N. T. Islam, C. C. W. Lim, C. Cahall, J. Kim, and D. J. Gauthier, Provably secure and high-rate quantum key distribution with time-bin qudits, *Science Advances* **3**, e1701491 (2017), <https://www.science.org/doi/pdf/10.1126/sciadv.1701491>.
 - [30] K. W. Chan, J. P. Torres, and J. H. Eberly, Transverse entanglement migration in hilbert space, *Phys. Rev. A* **75**, 050101 (2007).
 - [31] J. Schneeloch and J. C. Howell, Introduction to the transverse spatial correlations in spontaneous parametric

down-conversion through the biphoton birth zone, *Journal of Optics* **18**, 053501 (2016).

- [32] M. P. Almeida, S. P. Walborn, and P. H. Souto Ribeiro, Experimental investigation of quantum key distribution with position and momentum of photon pairs, *Phys. Rev. A* **72**, 022313 (2005).
- [33] C. H. Bennett, G. Brassard, and N. D. Mermin, Quantum cryptography without bell's theorem, *Phys. Rev. Lett.* **68**, 557 (1992).
- [34] L. Sheridan and V. Scarani, Security proof for quantum key distribution using qudit systems, *Phys. Rev. A* **82**, 030301 (2010).
- [35] V. Vidyapin, Y. Zhang, D. England, and B. Sussman, Characterisation of a single photon event camera for quantum imaging, *Scientific Reports* **13**, 1009 (2023).
- [36] B. G. Oripov, D. S. Rampini, J. Allmaras, M. D. Shaw, S. W. Nam, B. Korzh, and A. N. McCaughan, A superconducting nanowire single-photon camera with 400,000 pixels, *Nature* **622**, 730 (2023).
- [37] G. C. G. Berkhout, M. P. J. Lavery, J. Courtial, M. W. Beijersbergen, and M. J. Padgett, Efficient sorting of orbital angular momentum states of light, *Phys. Rev. Lett.* **105**, 153601 (2010).
- [38] M. P. J. Lavery, D. J. Robertson, G. C. G. Berkhout, G. D. Love, M. J. Padgett, and J. Courtial, Refractive elements for the measurement of the orbital angular momentum of a single photon, *Opt. Express* **20**, 2110 (2012).
- [39] H. Larocque, J. Gagnon-Bischoff, D. Mortimer, Y. Zhang, F. Bouchard, J. Upham, V. Grillo, R. W. Boyd, and E. Karimi, Generalized optical angular momentum sorter and its application to high-dimensional quantum cryptography, *Opt. Express* **25**, 19832 (2017).
- [40] N. K. Fontaine, R. Ryf, H. Chen, D. T. Neilson, K. Kim, and J. Carpenter, Laguerre-gaussian mode sorter, *Nature communications* **10**, 1865 (2019).
- [41] M. Mirhosseini, O. S. Magaña-Loaiza, M. N. O'Sullivan, B. Rodenburg, M. Malik, M. P. J. Lavery, M. J. Padgett, D. J. Gauthier, and R. W. Boyd, High-dimensional quantum cryptography with twisted light, *New Journal of Physics* **17**, 033033 (2015).
- [42] A. Mair, A. Vaziri, G. Weihs, and A. Zeilinger, Entanglement of the orbital angular momentum states of photons, *Nature* **412**, 313 (2001).
- [43] A. D'Errico, F. Hufnagel, F. Miatto, M. Rezaee, and E. Karimi, Full-mode characterization of correlated photon pairs generated in spontaneous downconversion, *Opt. Lett.* **46**, 2388 (2021).
- [44] F. Bouchard, R. Fickler, R. W. Boyd, and E. Karimi, High-dimensional quantum cloning and applications to quantum hacking, *Science Advances* **3**, e1601915 (2017), <https://www.science.org/doi/pdf/10.1126/sciadv.1601915>.
- [45] A. Zhao, M. van Beuzekom, B. Bouwens, D. Byelov, I. Chakaberia, C. Cheng, E. Maddox, A. Nomerotski, P. Svihra, J. Visser, V. Vrba, and T. Weinacht, Coincidence velocity map imaging using tpx3cam, a time stamping optical camera with 1.5 ns timing resolution, *Review of Scientific Instruments* **88**, 113104 (2017).

SUPPLEMENTARY

A. Experimental setup

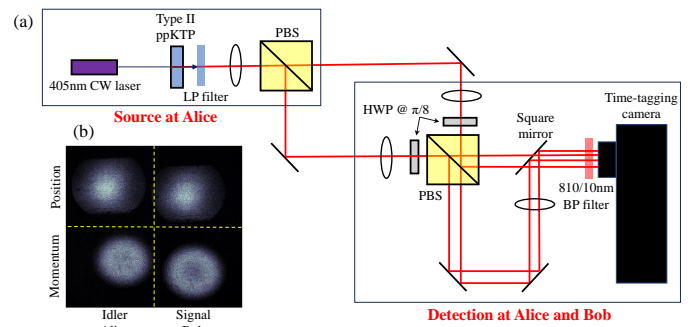


FIG. 4. **Experimental setup**(a) Experimental setup for position-momentum QKD. LP-filter: long-pass filter, BP-filter: band-pass filter, PBS: polarizing beam-splitter, HWP: half-wave plate (b) Image captured on camera of the position and momentum planes of SPDC.

The experimental setup for demonstrating high-dimensional QKD via position-momentum entangled photons is shown in Figure 4(a). Due to possessing only a single time-tagging camera (TPX3CAM) [25, 26], it is used as the detector for both Alice and Bob for this experimental demonstration. In practice, at least 2, preferably 4, such cameras should be used, one for each party (for 2 cameras) or one for each MUB at each party (for 4 cameras).

Source at Alice: Position-momentum entangled photon pairs with orthogonal polarization are generated at a rate of approximately 13×10^6 photon pairs per second by pumping a 1 mm thick Type-II ppKTP crystal with a 40mW collimated 405 nm CW laser having a beam width of 0.28 mm FWHM at the crystal plane. The orthogonally polarized photons are separated using a polarizing beam-splitter (PBS) with one photon kept by Alice and the partner sent to Bob.

Detection at Alice and Bob: The polarization of each photon is rotated by $\pi/4$ using half-wave plates (HWP), so at the PBS each photon will have a 50% probability of being detected in one of the two MUBs, position or momentum. A 50:50 beamsplitter can be used here instead for the same effect, we used a PBS combined with HWPs to have control over the photon splitting ratio. A square mirror is used to recombine the four beams onto the camera, where the two beams to be measured in the position plane pass over the mirror unaffected, and the two beams to be measured in the momentum plane are reflected by the mirror onto the camera. As seen in Figure 4(b), the camera sensors are slit into four quadrants, with the left two quadrants used as the detector for ALice's MUBS and the right two quadrants used as the detector for Bob's MUBS.

Imaging lenses were used to image the near-field (position plane) of the ppKTP crystal onto the camera with a magnification of ~ 5 times and image the far-field (momentum plane) onto the camera with a demagnification of ~ 5 times.

A singles rate (number of detected signal or idler photons) of $758 \times 10^3/\text{s}$ and a coincidence rate of $38 \times 10^3/\text{s}$

was measured by the camera. The background, consisting of environmental background and detector dark counts, is measured to be around $91 \times 10^3/\text{s}$. Together, this gives a total detection efficiency of $\sim 5.3\%$ for the experimental setup. The detection efficiency of the TPX3CAM is 8% [35], details on data processing of the raw camera data can be found in [35, 45].